Numerical Investigation and Uncertainty Analysis of Eastern China's Large-Scale Urbanization Effect on Regional Climate

Jiping QUAN[1], Yongkang XUE[2,3*], Qingyun DUAN[4], Zhenxin LIU[5], Keith W. OLESON[6], and Ye LIU[2]

1 *Institute of Urban Meteorology, China Meteorological Administration, Beijing* 100089, *China*
2 *Department of Geography, University of California, Los Angeles, CA* 90095, *USA*
3 *Department of Atmospheric & Oceanic Sciences, University of California, Los Angeles, CA* 90095, *USA*
4 *State Key Laboratory of Hydrology–Water Resources and Hydraulic Engineering, College of Hydrology and Water Resources, Hohai University, Nanjing* 210098, *China*
5 *School of Environmental Science and Engineering, Nanjing University of Information Science & Technology, Nanjing* 210044, *China*
6 *National Center for Atmospheric Research, Boulder, CO* 80307, *USA*

(Received February 18, 2021; in final form September 29, 2021)

ABSTRACT

Eastern China has experienced rapid urbanization during the past four decades, and it is necessary to understand the impacts of the urbanization on the regional climate. Previous simulations with either regional climate models (RCMs) or general circulation models have produced inconsistent and statistically non-significant urbanization effects on precipitation during the East Asian summer monsoon. In the studies with RCMs, reanalysis data were used as the lateral boundary conditions (LBCs) for both urban and non-urban experiments. Since the same LBCs may limit the urbanization effect, in this study, the Weather Research and Forecasting (WRF) model nested within the Global Forecast System (GFS), both of which were coupled with an urban canopy model, were used to explore the urbanization effect over eastern China. The WRF's LBCs in the runs with/without urbanization were provided by the corresponding GFS runs with/without urbanization. The results showed a significant decrease in precipitation over North China, mainly due to a marked decrease in evaporation and the divergence induced by the reduced latent heating in the mid and upper atmosphere, from the experiment with urbanization. Meanwhile, to the north and south of the large-scale urbanization areas, especially to the south of the Yangtze River, precipitation increased significantly due to large-scale urbanization-induced circulation change. With the same LBCs for the WRF runs with/without urbanization, the urbanization effects were limited only to urban and nearby areas; no significant change was found to the south of the Yangtze River, since the same LBCs hampered the effects of urbanization on large-scale circulation. In addition, this study demonstrated that the urban fraction may be a key factor that affects the intensity of the urbanization effect within the urban areas.

Key words: urbanization effect, regional climate model, uncertainty analysis, lateral boundary condition, urban fraction

Citation: Quan, J. P., Y. K. Xue, Q. Y. Duan, et al., 2021: Numerical investigation and uncertainty analysis of eastern China's large-scale urbanization effect on regional climate. *J. Meteor. Res.*, **35**(6), 1023–1040, doi: 10.1007/s13351-021-1033-y.

1. Introduction

Land use and land cover (LULC) change plays an important role in regional climate by altering the energy and moisture exchange between the land surface and the atmosphere (Xue, 1996; Xue et al., 2004). With the rapid urbanization in the past few decades in eastern China, especially in the Beijing–Tianjin–Hebei (BTH; around 38°–40.5°N, 115°–118°E), Yangtze River Delta (YRD; around 30°–32.5°N, 119°–122°E), and Pearl River Delta (PRD; around 22.5°–23.5°N, 112.5°–114.5°E) regions, all of which are outlined in Fig. 1d, understanding the climatic effects of urbanization-induced LULC change has become a necessity. The East Asian summer monsoon is

Supported by the National Key Research and Development Program of China (2018YFC1507801), National Science Foundation of U.S. (AGS-1419526), Beijing Natural Science Foundation (8204061), Beijing–Tianjin–Hebei Collaborative Innovation Community Construction Project (19245419D), and State Key Laboratory of Earth Surface Processes and Resource Ecology (2017-KF-05).

*Corresponding author: yxue@geog.ucla.edu

one of the major climate features in eastern China (Xue et al., 2004), and therefore we focus mainly on the effects of urbanization on the summer monsoon in this paper.

Researchers have extensively explored the effects of urbanization based on observational data. In particular, the urban heat island (UHI) effect (Oke, 1979), which is the phenomenon whereby temperature in urban areas is higher than that in the surrounding rural areas, has been confirmed by observational data from satellites (Jin et al., 2005; Peng et al., 2012; Zhou et al., 2015) as well as ground stations (Wang et al., 1990; Wu and Yang, 2013; Liao et al., 2017).

Although there is consensus on the UHI effect, the urban effect on precipitation during the warm season is uncertain. Some studies, based on comparing the precipitation over urban areas and their surrounding rural areas, have suggested an urbanization-induced increase in precipitation over urban areas (Song et al., 2014; Li et al., 2015). Such changes, however, have been found to be statistically non-significant. Moreover, there may be some caveats to the results. For instance, the dynamic growth and intensity of the urbanization were not taken

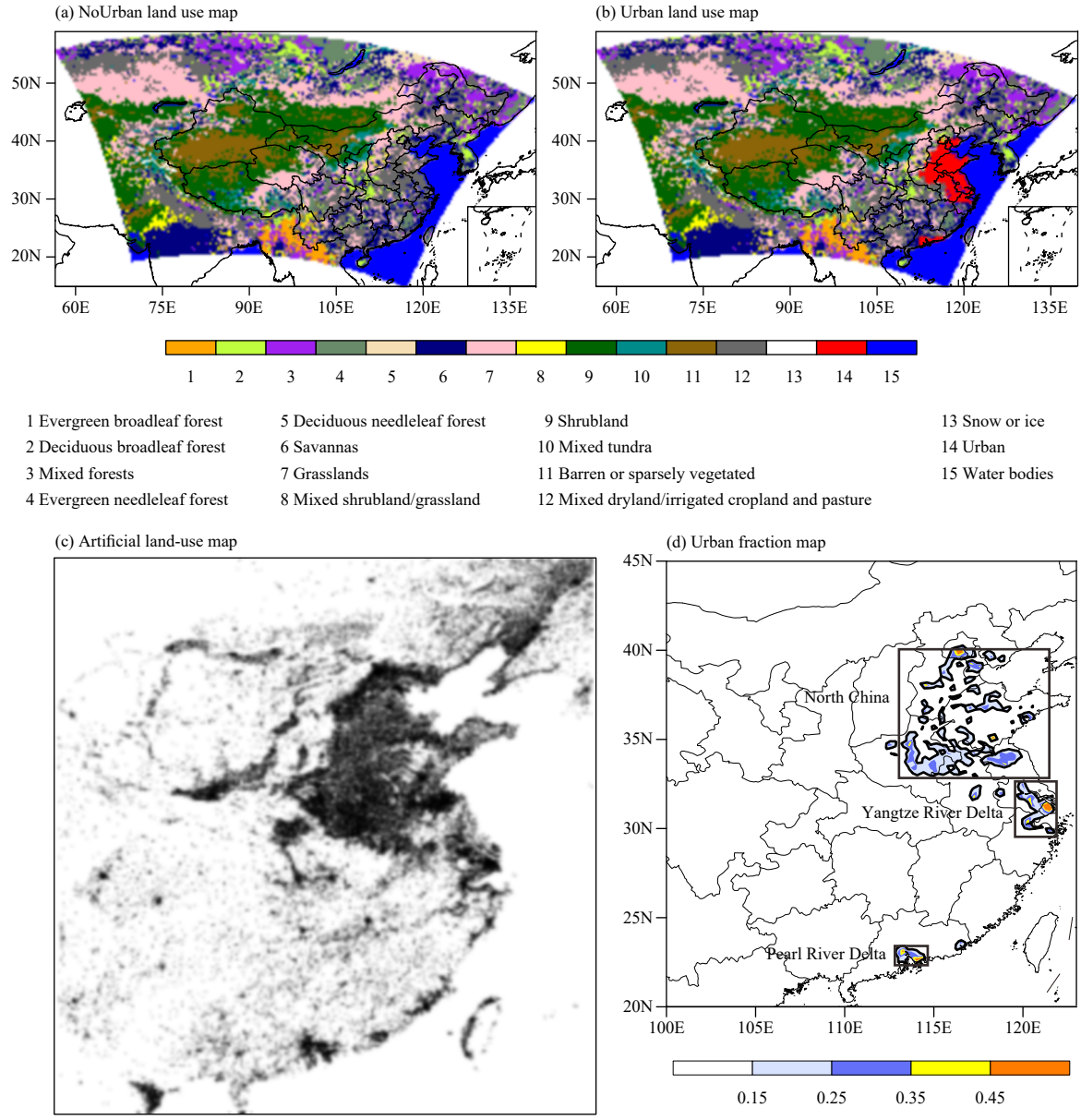

Fig. 1. (a) The NoUrban LULC map used in the WRF experiment without urbanization. (b) The Urban LULC map used in the WRF experiments with urbanization. (c) Artificial land-use map for eastern China, the data for which were from the Global Artificial Land Surface Dataset at 30-m resolution (2010) (Chen et al., 2014). (d) Urban fraction map estimated based on the artificial land-use map shown in (c). The regions encircled in black indicate the urban areas where the urban fraction is greater than 0.15.

into consideration, and when those specific urban characteristics have been considered, different results emerged (Kaufmann et al., 2007; Niyogi et al., 2017). For example, by considering the urban growth in each year in the Pearl River Delta region with analysis based on the notion of Granger causality, no causal relationship was found between urbanization and precipitation during summer (Kaufmann et al., 2007). Meanwhile, taking into account the intensity of urbanization over the eastern United States, it was found that urban centers experienced a decrease in rainfall amounts, but areas located in the urban periphery exhibited a higher probability of heavy rainfall (Niyogi et al., 2017). Another study also showed that the impact of urbanization and forest cover change on precipitation was inconclusive (positive, neutral, and negative; Cao et al., 2020).

Since the observational data in urban and surrounding areas are normally composed of effects caused by many factors in addition to urbanization, such as aerosol conditions, climate variability and change, anthropogenic heat release, etc., it is hard to isolate the effects of urbanization from other factors. Accordingly, climate models have to be applied to identify the effects of urbanization.

Both regional climate models (RCMs) and general circulation models (GCMs) have been employed to explore the effects of urbanization on the East Asian summer monsoon. In general, such numerical experiments have used two land-use maps: one being before and the other after the urbanization in the GCM and RCM for non-urban and urbanization experiments, respectively. By comparing the results from the runs with the different land-use maps, the results consistently show urban-induced warming over urban areas (Miao et al., 2008; Zhang et al., 2010; Wang et al., 2013; Cao et al., 2016; Ma et al., 2016; Liao et al., 2017; Zhao and Wu, 2017), confirming the UHI effect.

In addition, the effects of urbanization on precipitation are again rather divergent in model simulations. Studies with the Community Atmosphere Model and Community Land Model for urbanization effects over East China indicate that precipitation has decreased over the large-scale urbanization area and increased to the south (Ma et al., 2016); however, the decreases over the large-scale urbanization areas are statistically non-significant, probably because of the coarse horizontal model resolution.

Studies with RCMs [(for example, the Weather Research and Forecasting (WRF) model with the Noah land surface model)] have mainly focused on the effects of urbanization over the three main urban agglomeration areas in eastern China (BTH, YRD, and PRD). The urban effects on precipitation over these urban areas are mostly statistically non-significant and not always consistent among RCMs (Zhang et al., 2010; Cheng and Chan, 2012; Wang et al., 2012; Zhang et al., 2014; Zhao and Wu, 2017). For each urban agglomeration area (BTH, YRD, or PRD), most simulations show an increase in precipitation, but some show a decrease.

It is noteworthy that all simulations with RCMs have used reanalysis data as the lateral boundary conditions (LBCs) for both urban and non-urban experiments. Since RCMs are designed to preserve the large-scale circulation features in the imposed LBCs and to add more information at a finer scale, the same LBCs may dampen the effects of imposed perturbations in the sensitivity experiment (Xue et al., 2014). In this study, we used the NCEP Global Forecast System (GFS) nested with the Advanced Research version of WRF (WRF-ARW), both of which were coupled with the Simplified Simple Biosphere Model (SSiB; Xue et al., 1991; Sun and Xue, 2001) and an urban canopy model (Oleson et al., 2008; Liu, 2013), to explore the effects of urbanization in East China. In one set of the experiments, the RCM's LBCs with/without urbanization were specified with the corresponding GFS LBCs with/without urban LULC change. In addition, we also ran WRF with/without urbanization experiments with the same LBCs from the GFS non-urban experiments. By comparing the differences in the urbanization effects with the different LBCs and the same LBCs, the latter of which is the approach used in almost all previous RCM studies on the effects of urbanization, the uncertainty in the urbanization effects due to LBCs was assessed.

In addition, another factor that may cause large uncertainty in assessing the urbanization effects that is the urban fraction in the urban canopy model. This study also tested the effects of two approaches in specifying the urban fraction, both of which have been widely employed in previous studies with RCMs. One assigns a constant for the urban fraction over all of the urban areas (such as 0.9 or 0.95; Lo et al., 2007; Zhang et al., 2010; Cheng and Chan, 2012; Wang et al., 2012; Zhang et al., 2014); while in the other approach, the urban fraction at each urban grid cell is calculated more realistically based on urban land-cover datasets (Hu et al., 2015; Jia et al., 2015; Zhao and Wu, 2017).

2. Methods

2.1 *Model description*

The NCEP's GFS (Saha et al., 2010), as well as the NCNR's WRF-ARW, version 3.7 (Skamarock et al., 2008), were employed in this study. A single-layer urban can-

opy model (Oleson et al., 2008; Liu, 2013) was coupled to the SSiB land-surface model in the GFS and WRF models (Xue et al., 1991; Sun and Xue, 2001). GFS/SSiB and WRF/SSiB have been used extensively for studies in East Asia (Xue et al., 2004, 2010, 2018; Sato and Xue, 2013; Li et al., 2016). The performances of these models in capturing the major climate features in East Asia have been extensively validated in these studies.

In total, there are 18 input parameters in the urban model to describe the morphological, radiative, and thermal characteristics of the urban model (Table 1). The values of the parameters were assigned based on global databases of urban extent and characteristics that can be utilized to simulate urban systems on a global scale (Jackson et al., 2010). In addition, we also specified some settings for the urban model in eastern China based on related literature (Wang and Jiang, 2009; Zhang et al., 2010; Cheng et al., 2011; Miao et al., 2012; Ding, 2013; Meng and Dai, 2013).

In addition to the SSiB land-surface model coupled with the urban-canopy model, the other parameterization schemes used for the WRF simulations (Li et al., 2016) included the Kain–Fritsch scheme (Kain, 2004) for cumulus processes, the WSM Single-Moment 6-class scheme (Hong and Lim, 2006) for microphysics processes, the Community Atmosphere Model scheme for short- and longwave radiation processes (Collins et al., 2004), and the Yonsei University scheme (Hong et al., 2006) for planetary boundary layer processes.

2.2 *Land-use and land-cover maps*

The NoUrban LULC map (Fig. 1a) was generated with the default SSiB LULC map (Xue et al., 2004), in which there was no urban LULC. The Urban LULC map (Fig. 1b) was created by overlaying the NoUrban LULC map with the urbanization map, which was based on the 2010 Global Artificial Land Surface Dataset at 30-m resolution over eastern China (Fig. 1c; Chen et al., 2014; available at http://www.geodoi.ac.cn/). The Artificial Land Surface Dataset was developed based on data mining via the integration and analysis of 9907 scenes of the USA Landsat Thematic Mapper 5, Enhanced Thematic Mapper data, and 2640 scenes of China's Environmental Disaster Mitigation Satellite data in 2010 (Chen et al., 2017). Figure 1d shows three urbanization areas: two are the large-scale urban areas over the lowland plains of eastern China that cover the BTH and YRD regions, and the other one is in the PRD region of southern China.

For each grid cell in the urban area, only part of it was urban with an impervious surface. The other part was represented by the natural LULC in the NoUrban LULC map. The percentage of urbanization was specified by the urban fraction. The urban fractions in all of the urban experiments except for the GFS_Urban_ConsFrac and Urban1_ConsFrac experiments (Table 2, which will be discussed in Section 2.3) were estimated based on the 2010 Global Artificial Land Surface Dataset at 30-m resolution (Fig. 1c; Chen et al., 2014), and are consistent with those found by satellite images (Hu et al., 2015). Three major urbanization areas where the urban fractions are greater than 0.15 are shown (Fig. 1d): the area over eastern China (including the BTH area, YRD area, and PRD area); the latter two areas are far smaller than the former one. In the following analyses, some isolated urban areas will be smoothed and only the three major urbanization areas will be specified for clarity. The urban fractions in the GFS_Urban_ConsFrac and Urban1_ConsFrac experiments were set to a constant value of 0.4 (Table 2) based on the fraction of impervious surface over the BTH and YRD areas estimated by remote sensing observations (Cui et al., 2015; Han et al., 2015).

Table 1. Input data for the urban model

Parameter description	Value
Morphological characteristics	
Building height (m)	21
The fraction of building in unit urban area	0.35
Ratio of building height and street width	1.0
Radiative characteristics	
Surface albedo of building roof for visible light	0.17
Surface albedo of building roof for infrared light	0.37
Surface albedo of building wall for visible light	0.25
Surface albedo of building wall for infrared light	0.35
Surface albedo of impervious ground for visible light	0.13
Surface albedo of impervious ground for infrared light	0.16
Surface emissivity of roof	0.91
Surface emissivity of building wall	0.907
Surface emissivity of impervious road	0.91
Thermal characteristics	
Heat capacity of roof (J m^{-3} K^{-1})	554066.03
Heat capacity of wall (J m^{-3} K^{-1})	936188.98
Heat capacity of impervious road (J m^{-3} K^{-1})	1712294.74
Thermal conductivity of roof (J m^{-1} s^{-1} K^{-1})	0.08
Thermal conductivity of building wall (J m^{-1} s^{-1} K^{-1})	1.32
Thermal conductivity of impervious road (J m^{-1} s^{-1} K^{-1})	1.67

2.3 *Experimental design*

Three scenarios with the GFS (Table 2) were designed: (1) GFS_NoUrban, (2) GFS_Urban, and (3) GFS_Urban_ConsFrac. All of the settings for the three scenarios were the same, except for the LULC maps. GFS_NoUrban used the NoUrban LULC map; GFS_Urban used the Urban LULC map with the urban fraction for each grid cell estimated based on the 2010 Global Artificial Land Surface Dataset as discussed in Section 2.2 (similar to Fig. 1d, omitted); and GFS_Urban_ConsFrac used the Urban LULC map with a constant

Table 2. Experimental design

Model	Experiment	Resolution	Land use land cover		Lateral boundary condition	Simulation period
			Land use map	Urban fraction		
GFS	GFS_NoUrban	T126	NoUrban	N/A	N/A	30 Apr to 1 Aug
	GFS_Urban		Urban	Fig. 1d		2005–2014
	GFS_Urban_ConsFrac		Urban	0.4		
WRF	NoUrban	25 km	NoUrban	N/A	GFS_NoUrban	2 May to 1 Aug
	Urban1		Urban	Fig. 1d	GFS_Urban	2005–2014
	Urban2		Urban	Fig. 1d	GFS_NoUrban	
	Urban1_ConsFrac		Urban	0.4	GFS_Urban_ConsFrac	

urban fraction of 0.4 for each grid cell, which is slightly exaggerated with an average increase by about 0.27. Ten cases from 2005 to 2014 were simulated for each scenario, with each being integrated from 30 April to 1 August. The horizontal resolution was T126. The initial conditions were from CFSv2 reanalysis data (Saha et al., 2010), and the sea surface temperature and sea ice data were from the ERA-Interim reanalysis dataset of the ECMWF (Dee et al., 2011).

Four scenarios with the WRF model (Table 2) were designed: (1) NoUrban, (2) Urban1, (3) Urban2, and (4) Urban1_ConsFrac. NoUrban was the control experiment. It used the NoUrban LULC map (Fig. 1a) and LBCs from GFS_NoUrban. The other three experiments were the sensitivity experiments. All of them used the Urban LULC map (Fig. 1b). However, the LBCs and urban fractions were different. The urban fractions in the Urban1 and Urban2 experiments (Fig. 1d) were estimated based on the 2010 Global Artificial Land Surface Dataset (Fig. 1c)—similar to the settings for GFS_Urban, but with different LBCs. Urban1 used the LBCs from GFS_Urban, while Urban2 used the LBCs from GFS_NoUrban. The LBCs in Urban1_ConsFrac were from GFS_Urban_ConsFrac, and the urban fraction used in Urban1_ConsFrac was 0.4, which was the same as the setting in GFS_Urban_ConsFrac.

The results with the Urban LULC map minus those with the NoUrban LULC map indicated the urbanization effects due to urban LULC change (Fig. 2). GFS_Urban minus GFS_NoUrban indicated the urbanization effects with GFS simulations. GFS_Urban_ConsFrac minus GFS_NoUrban also indicated the urbanization effects with GFS simulations, but the urban fraction was constant (0.4) over all of the urban areas. Urban1 minus NoUrban indicated the WRF-simulated urbanization effects. Urban2 minus NoUrban indicated the WRF-simulated urbanization effects with the same LBCs. Urban1_ConsFrac minus NoUrban indicated the WRF-simulated urbanization effects with a constant urban fraction of 0.4. Therefore, the difference between Urban1 and Urban2 showed the uncertainty in the effect of urbanization due to the LBCs, and the difference between Urban1 and Urban1_ConsFrac showed the uncertainty due to the specification of urban fraction.

3. Results

The analyses in this section focus on the mean of June and July averaged over 10 yr from the WRF-simulated urbanization effects with the control and sensitivity runs using the LBCs from the corresponding GFS control and sensitivity runs, respectively, as well as the mechanisms

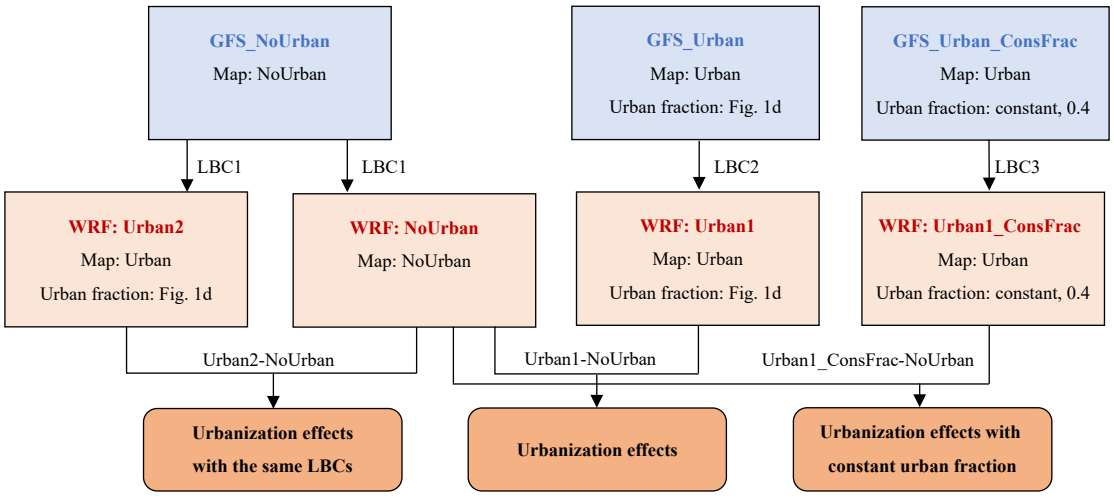

Fig. 2. Experimental design and urbanization effects.

involved. These results are also compared to those obtained from the control and sensitivity runs with the same LBCs. The sensitivity of the urbanization effects to urban fractions is also discussed.

3.1 *WRF-simulated urbanization effects with different LBCs*

In this section, the NoUrban run is used as the control run, the Urban1 run is used as the sensitivity run, and their differences are used to assess the urbanization effect.

3.1.1 *WRF-simulated urbanization effects on energy balance and surface temperature*

With urbanization, the natural surface is replaced by artificial land surfaces with different albedo and emissivity. Meanwhile, the urban canyon traps the incoming shortwave and outgoing longwave radiation. The surface albedo and emissivity are highly dependent on the radiative characteristics of building rooves, building walls, and impervious roads. These urban surface parameters values in this study were specified based on global databases of urban extent and characteristics (Jackson et al., 2010) and related literature (Wang and Jiang, 2009; Zhang et al., 2010; Cheng et al., 2011; Miao et al., 2012; Ding, 2013; Meng and Dai, 2013). Our simulations also produced very small changes in albedo and emissivity (not shown), generally consistent with the results indicated by the Global Land Surface Satellite (GLASS) products (Liu et al., 2013; Cheng et al., 2014).

The surface incoming shortwave radiation flux (Fig. 3a) increases significantly over the area around 32.5°–40.5°N, 112°–119°E, which covers the BTH and its surrounding areas and is referred to as North China in this paper, as well as over the south coastal PRD area, probably due to the decrease in low-level cloud cover (Fig. 4a). Meanwhile, the incoming shortwave radiation decreased in the northern part of North China, over the YRD, and to the south of the Yangtze River, where low- and medium-level cloud cover increase (Fig. 4).

The surface net shortwave radiation flux (Fig. 3b), which is positive downward, increased, and decreased accordingly by about 3–15 W m^{-2} in the areas with reduced and elevated cloud, respectively. However, the surface net longwave radiation flux (Fig. 3c), which is positive downward, decreased by about 10–30 W m^{-2} over all of the urban areas owing to reduced incoming longwave radiation and high surface temperatures. Since the decrease in surface net longwave radiation flux was larger than the increase in surface net shortwave radiation flux, the surface net radiation flux (Fig. 3d) decreased by about 3–20 W m^{-2} over North China and 3–9 W m^{-2} over the PRD. Over the YRD, both the surface net shortwave radiation flux and the longwave radiation flux decreased; the surface net radiation flux decreased by about 15–30 W m^{-2}.

The impervious surfaces in the urban areas along with the lower surface net radiation flux reduce the evaporation/latent heat flux from the land surface (Fig. 5a). The decrease in surface wind speed due to high surface roughness length is another factor that contributed to the decrease in surface evaporation, which will be addressed in detail in Section 3.1.2. The maximum reduction in latent heat flux over the urban areas reached more than 30 W m^{-2}, which was larger than the reduction in surface net radiation flux. As a result of the surface energy balance, the surface sensible heat flux and ground heat flux increase (Figs. 5b, c).

Consistent with the increased surface ground heat flux and sensible heat flux, the surface skin temperature rose significantly over the urban areas (Fig. 6a), indicating a UHI effect. The increases in surface temperature were about 0.2–1°C over North China and the PRD, and 0.2–0.6°C over the YRD, which was the weakest among the three urbanization clusters. The 2-m air temperature there also showed a very similar increase. The simulated intensity of the UHI effect was consistent with the observed one. Based on station data in Beijing, Yan et al. (2016) suggested that the intensity of the annual average UHI is about 1–1.5°C, and Yang et al. (2013) suggested the intensity of the UHI in summer is about 0.92°C. Since the effects of anthropogenic heat release in the urban areas were not taken into consideration here (e.g., the heat emissions of air conditioning, vehicles, etc.), the simulated UHI intensity could be a little weaker than observed, and its spatial heterogeneity characteristics could be different from those observed, which indicates that the urbanization-induced warming in summer is strongest in the YRD among the three urbanization clusters in eastern China (Wu and Yang, 2013).

To the south of the Yangtze River, the decrease in surface net shortwave radiation flux was larger than the increase in surface net longwave radiation flux; thus, the surface net radiation flux decreases by about 3–15 W m^{-2} (Fig. 3). The reductions in surface latent heat flux were smaller compared to the areas with urbanization (Fig. 5). As such, the surface temperature decreased significantly, by about 0.2–0.6°C (Fig. 6a).

3.1.2 *WRF-simulated urbanization effects on precipitation and circulation*

The difference between the Urban1 and No-urban runs show a remarkably dry belt over North China (Fig. 6b),

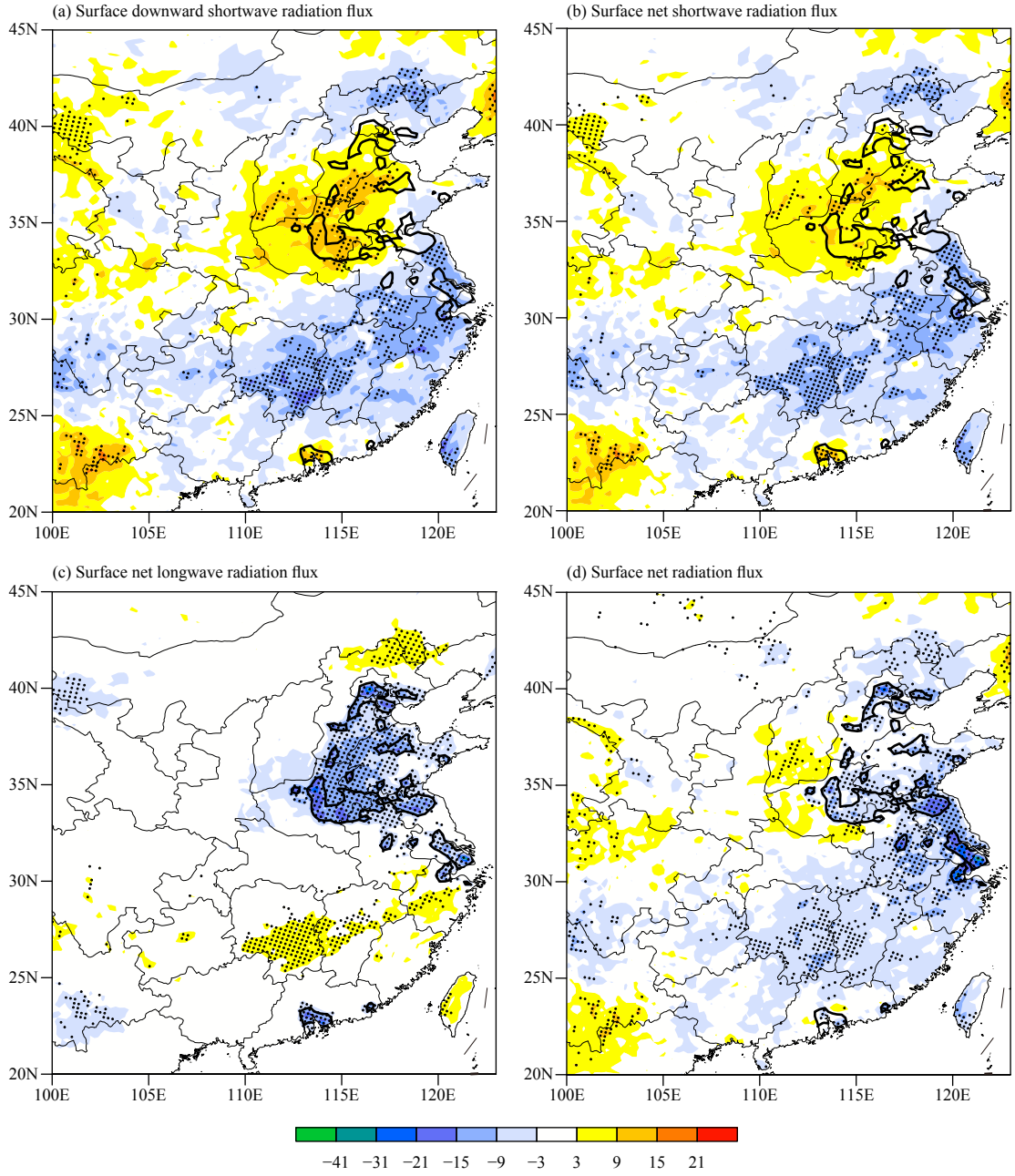

Fig. 3. WRF-simulated June–July urbanization effects on (a) surface downward shortwave radiation flux (W m^{-2}), (b) surface net shortwave radiation flux (W m^{-2}), (c) surface net longwave radiation flux (W m^{-2}), and (d) surface net radiation flux (W m^{-2}). Black dots indicate statistically significant areas at the 90% confidence level according to a *t*-test. The anomalous regions encircled in black indicate urban areas where the urban fraction is greater than 0.15. Some isolated urban areas are smoothed for clarity.

where precipitation is decreased significantly by about 1.5–3.5 mm day^{-1}. The results also show three wet belts: the north of North China, north of the YRD, and south of the Yangtze River. Precipitation increased significantly by about 0.5–3.5 mm day^{-1} over the north of North China, and by about 1.5–4.5 mm day^{-1} over the north of the YRD and to the south of the Yangtze River (Fig. 6b).

The reduction in precipitation in North China was consistent with the reduction there in surface latent heat flux (Fig. 5a) and descending motion (Fig. 7a), which were mainly related to the reduced atmospheric heating induced by the changes in surface characteristics and reduced surface latent heat flux—similar to the discussion in Xue (1996). With the decrease in surface evaporation induced by the urbanization in North China, latent heating in the mid and upper atmosphere was reduced, leading to a local cooling in the atmospheric layers, and thus a relative subsidence that contributed to the decrease

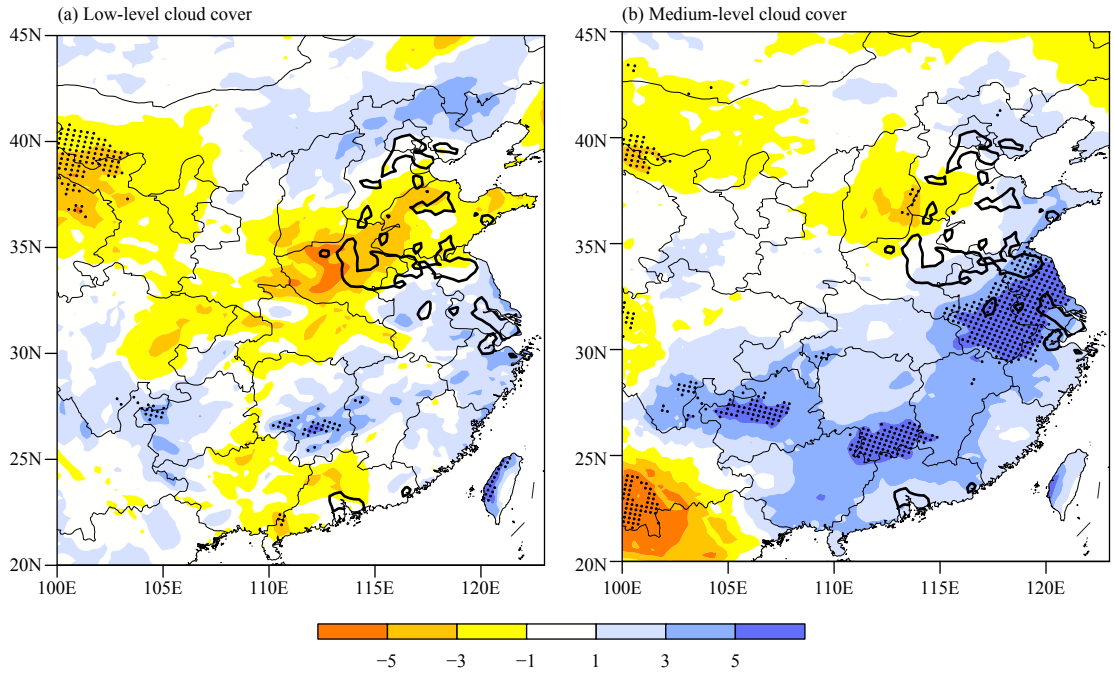

Fig. 4. WRF-simulated June–July urbanization effects on (a) low-level cloud cover (%) and (b) medium-level cloud cover (%). Black dots indicate statistically significant areas at the 90% confidence level according to a *t*-test. The anomalous regions encircled in black indicate urban areas where the urban fraction is greater than 0.15. Some isolated urban areas are smoothed for clarity.

there in low-level cloud cover (Fig. 4).

Due to the reduced latent heating in the mid and upper atmosphere, after the meridional temperature gradient reaches a peak near 32°N, roughly in the southern periphery of North China, it decreases to the north (Fig. 7b, averaged over 112°–119°E). The westerly wind anomaly reaches a peak at 32°N and an easterly wind anomaly appears to the north of 36°N (Fig. 7c), indicating a southward movement of the subtropical upper jet and the rainfall band (Fig. 6b). After analyzing the relationships between the subtropical upper jet and the changes in precipitation using NCEP reanalysis data and other observations, Du et al. (2009) suggested that the southward movement of the East Asian subtropical westerly jet is associated with more precipitation in the south and less precipitation in the north of East China.

With the anomalous subsidence produced in North China, because of the atmospheric mass balance as shown in the continuity equation, in the lower atmosphere, a southward atmospheric movement is induced to the south of the large-scale urbanization area, which tends to slow down the northward movement of the monsoonal flow. Moreover, the urban surface also creates barrier blocking/slowing of the northward monsoonal airflow at the lower levels. After urbanization, the surface roughness over the urban areas is increased (Fig. 8a) due to the presence of buildings, which imposed strong drag to slow down the wind in the surface layer (Xue et al., 1990). The wind speed at 10 m is weakened by about 0.2–0.4 m s^{-1} over the urban areas (Fig. 8b), consistent with observations over East China (Wu et al., 2016; Li et al., 2017; Zha et al., 2017; Liu et al., 2018).

The weakening of the northward monsoonal flow (Fig. 8c) and associated divergence in North China are the result of high surface roughness length, enhanced descending motion, and a southward shift of the subtropical upper jet. As such, anomalous convergence was produced to the south of the large-scale urbanization area. Consequently, precipitation is enhanced to the south of the large-scale urbanization area, and the low- and medium-level cloud cover increase.

Both the decrease in surface evaporation and increase in integrated moisture flux divergence contribute to the low precipitation over North China. The surface evaporation decreases by about 0.3–1.4 mm day^{-1} (Fig. 5a) and the integrated moisture flux divergence increases by about 1–4 mm day^{-1} (Fig. 8c). As a result, precipitation decreases significantly (Fig. 6b).

The divergence in North China induce a convergence to the north of 40°N, the north of the YRD, and the south of the Yangtze River, contributing to the three wet belts indicat above. Over the three wet belt areas, the substantial increase in integrated moisture flux convergence (Fig. 8c) is the dominant factor that lead to the increase

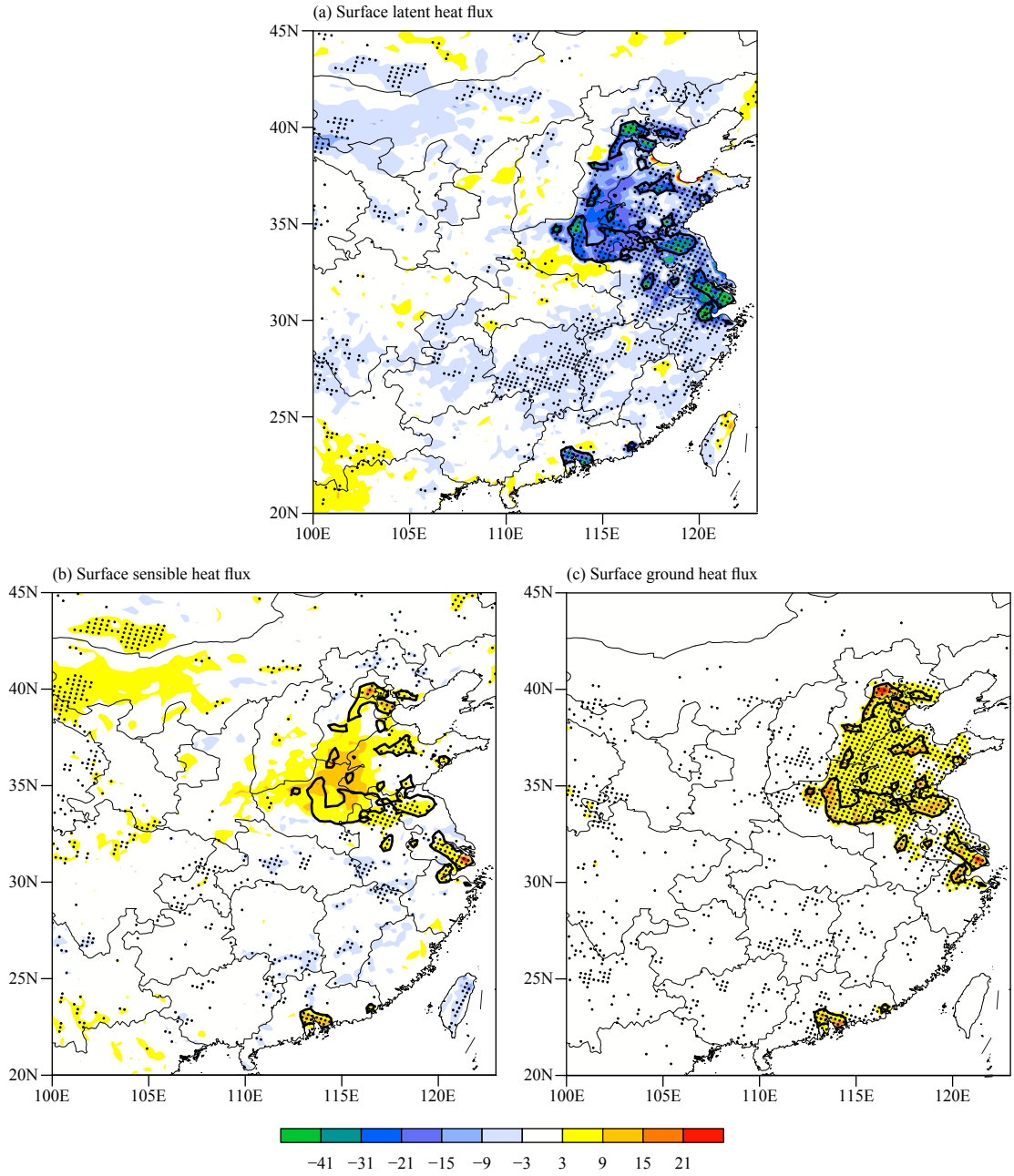

Fig. 5. WRF-simulated June–July urbanization effects on surface (a) latent heat flux (W m^{-2}), (b) sensible heat flux (W m^{-2}), and (c) ground heat flux (W m^{-2}). Black dots indicate statistically significant areas at the 90% confidence level according to a *t*-test. The anomalous regions encircled in black indicate urban areas where the urban fraction is greater than 0.15. Some isolated urban areas are smoothed for clarity.

in precipitation there. The increase in integrated moisture flux convergence there is dominant, at about 1–4 mm day^{-1} to the north of North China and to the south of the Yangtze River, where the reduction in surface evaporation is less than 0.3 mm day^{-1}. Over the north of the YRD, the increase in integrated moisture flux convergence is even higher, at about 2–6 mm day^{-1}.

Precipitation increased and decreased non-significantly over urban areas in Beijing and Tianjin, respectively—consistent with observational results that indicated no obvious effect on precipitation in the BTH city cluster (Jiang and Li, 2014). The precipitation changes over the YRD and PRD urban areas showed complex features. The precipitation decreased by about 0.5–1.5 mm day^{-1} over the southern part of the YRD, where the reduction in surface evaporation was dominant at about 1–1.4 mm day^{-1}. The enhanced precipitation in the northern part of the YRD was part of one of the wet precipitation belts discussed earlier. The anomalous precipitation pattern over the YRD showed consistency with the ana-

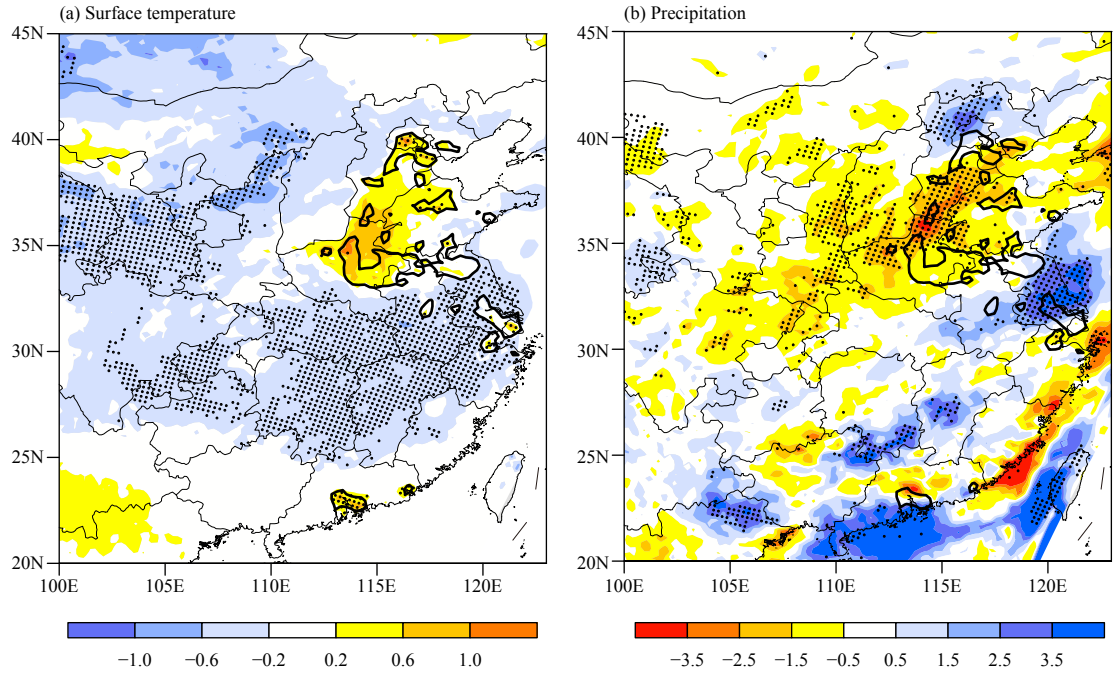

Fig. 6. WRF-simulated June–July urbanization effects on (a) surface skin temperature (°C) and (b) precipitation (mm day^{-1}). Black dots indicate statistically significant areas at the 90% confidence level according to a *t*-test. The anomalous regions encircled in black indicate urban areas where the urban fraction is greater than 0.15. Some isolated urban areas are smoothed for clarity.

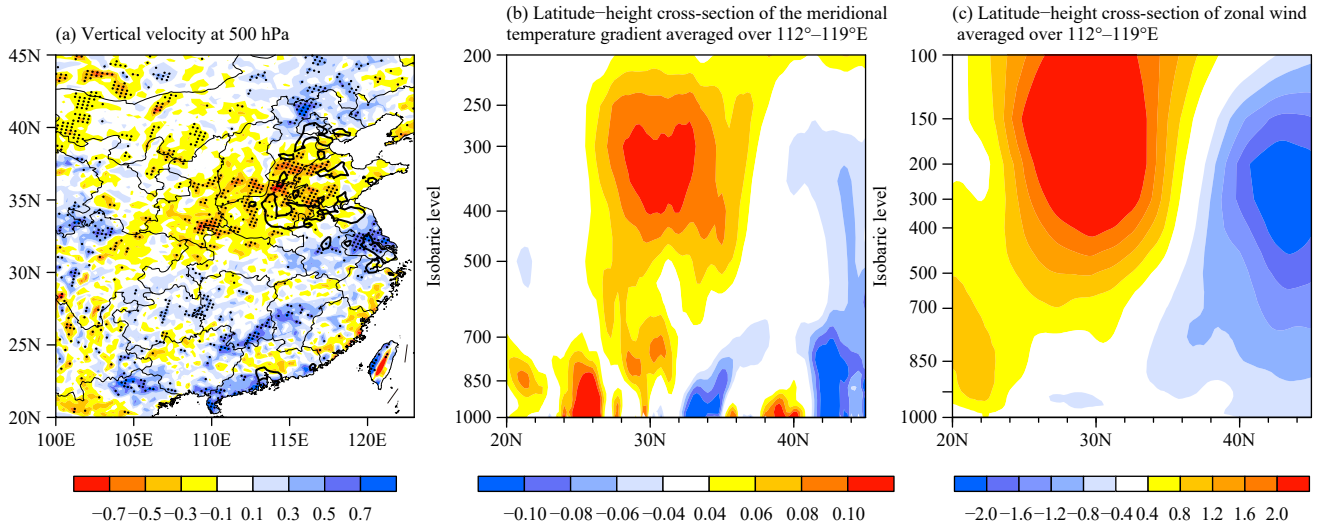

Fig. 7. WRF-simulated June–July urbanization effects on (a) vertical velocity at 500 hPa (cm s^{-1}), (b) the latitude–height cross-section of the meridional temperature gradient (K degree^{-1}) averaged over 112°–119°E, and (c) the latitude–height cross-section of zonal wind (m s^{-1}) averaged over 112°–119°E.

lysis using the high-resolution Climate Prediction Center Morphing technique precipitation product (CMORPH; Fu et al., 2019).

Precipitation over the PRD showed a non-significant decrease over the north and a non-significant increase over the south. These patterns of anomalous precipitation patterns are in line with previous simulation results, which showed a decrease and an increase in rainfall over the inland region and coastal region of the PRD urban area, respectively (Cheng and Chan, 2012). However, observational data suggest that there is no causal relationship between urbanization and summer precipitation over the PRD (Kaufmann et al., 2007).

For urban areas close to the ocean, sufficient water vapor in the atmosphere normally favors the thermal convection induced by the warming of the surface. As such,

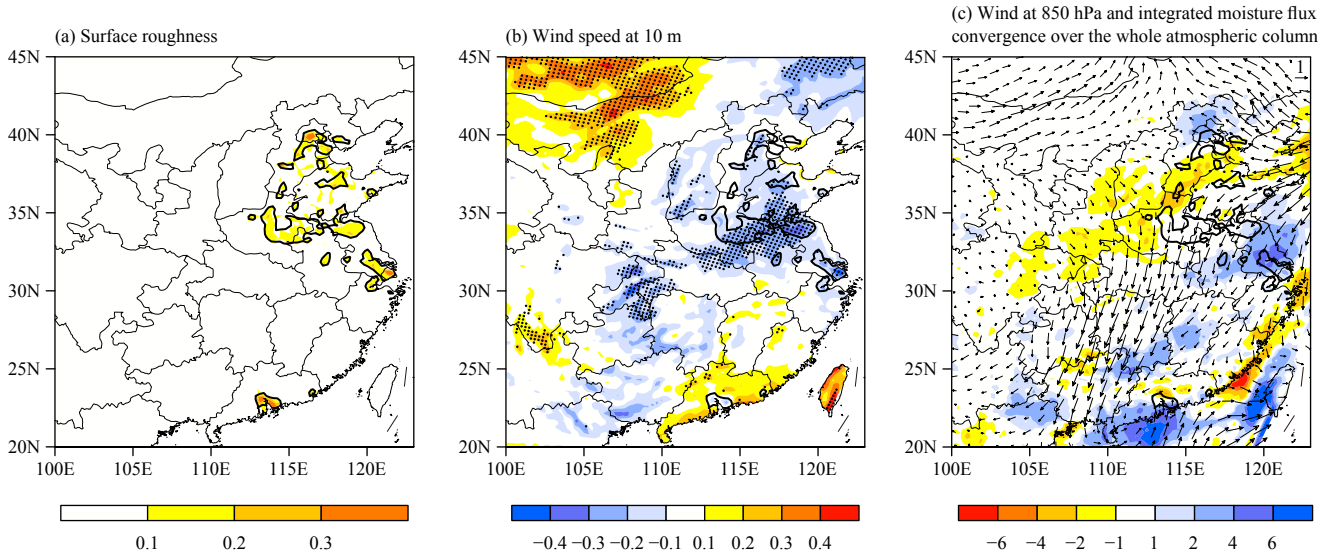

Fig. 8. WRF-simulated June–July urban effects on (a) surface roughness (m), (b) wind speed at 10 m (m s^{-1}), and (c) wind at 850 hPa and integrated moisture flux convergence over the whole atmospheric column (mm day^{-1}).

the increase or decrease in precipitation over these urban areas depends on whether the reduction in evapotranspiration or the increase in the moisture flux convergence dominates the processes, and normally displays complex precipitation-anomaly features.

3.2 *WRF-simulated urbanization effects with the same LBCs*

In this next part of the study, the NoUrban run was used as the control run and the Urban2 run, which used the same LBCs as the NoUrban run, was used as the sensitivity run. Their differences were used to assess the effects of urbanization under the same LBCs for both runs.

The results show significant warming of about 0.2–1.4°C over all three urban areas—warmer than that simulated with the different LBCs (Figs. 6a, 9a). In the Urban2 run, the changes in surface condition over the urban areas are the same as those in the Urban1 run. The urban-induced changes in surface latent heat flux and net radiation flux are also similar (not shown). Outside the urban areas, there were no changes in surface temperature around the YRD or to the south of the Yangtze River—different from the significant cooling simulated with the different LBCs, which is induced by the changes in large-scale circulation.

Compared to the results simulated with different LBCs (Fig. 6b), the effects of urbanization on precipitation (Fig. 9b) suggest a similar pattern over the urban and surrounding areas. One dry belt is apparent over North China, while two wet belts appear north of North China and over the north of the YRD area. However, the intensity of these two wet belts is weaker. Moreover, no significant changes in precipitation are found to the south of the Yangtze River. That said, the effect of urbanization on precipitation is similar only over urban areas with the same LBCs.

The significant differences in the response of surface temperature and precipitation outside the urban areas are the reason that there have been no striking changes in circulation in the runs with the same LBCs. Although the wind speed at 10 m decreases over most of the urban areas (not shown), similar to that simulated with different LBCs, there are no significant changes for the meridional temperature gradient (not shown) and zonal wind speed (not shown). No substantial shift in the subtropical jet is found (Fig. 10c).

The simulations with different LBCs dynamically downscaled the effects of the urbanization on circulation. However, the simulations with the same LBCs limited the effects of urbanization on circulation change because the basic principle of the RCM's design is to preserve the imposed large-scale circulation from the imposed LBCs (Xue et al., 2014). When the main pathway of the developing perturbation was through large-scale circulation change caused by the urbanization, the imposition of the same LBCs could hamper the necessary modification at a large scale, especially when the urbanization-induced large-scale circulation was not that strong. With the same LBCs, the large-scale circulation changes in the Urban2 run due to the effects of urbanization were largely restrained. The effects of urbanization on 200-hPa zonal wind simulated by the WRF with different LBCs are con-

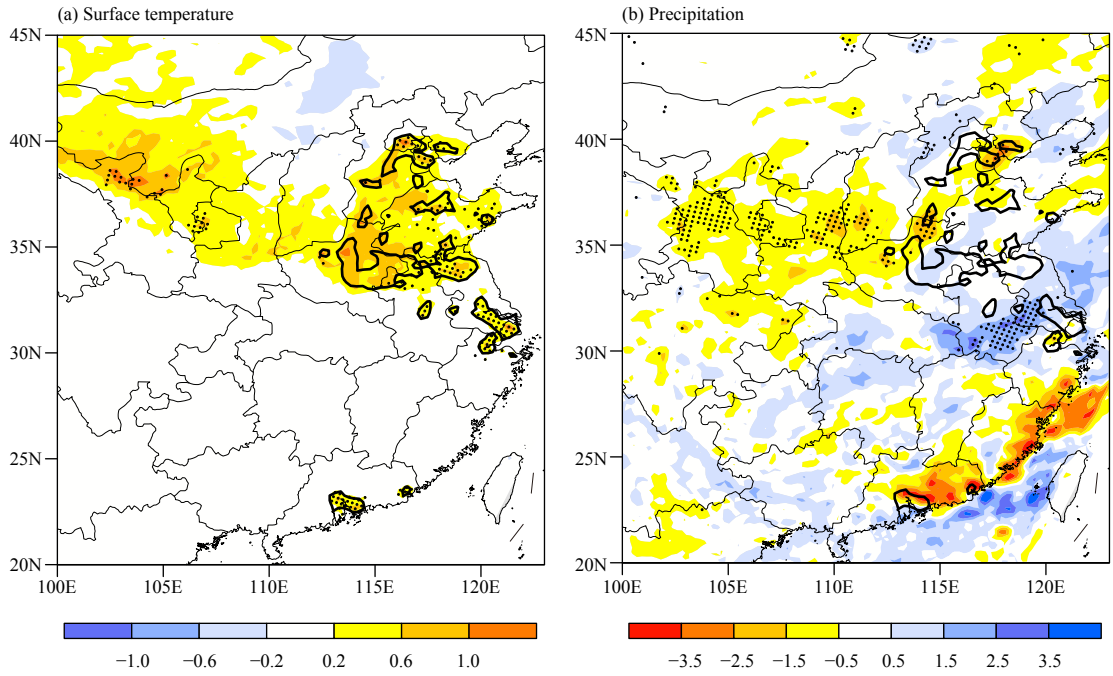

Fig. 9. WRF-simulated June–July urbanization effects on (a) surface temperature (°C) and (b) precipitation (mm day^{-1}) with the same LBCs. Black dots indicate statistically significant areas at the 90% confidence level according to a *t*-test. The anomalous regions encircled in black indicate urban areas where the urban fraction is greater than 0.15. Some isolated urban areas are smoothed for clarity.

sistent with the GFS results (Figs. 10a, b)—both showing stronger zonal wind near 30°N due to changes in the temperature gradient (Li et al., 2007). However, with the same LBCs, this process of thermal wind adjustment is compromised because of the same imposed large-scale circulation (Fig. 10c), which led to crucial differences in the RCM-simulated urbanization effects outside the urban areas between the runs with the same LBCs and those with different LBCs (Figs. 6, 9). The WRF results with different LBCs show cooling and a significant increase in precipitation outside the urbanization area, consistent with the GFS simulation (Fig. 6, see Fig. S1 in the supplemental material). However, the GFS results were statistically non-significant, demonstrating the added value in regional downscaling.

3.3 *Sensitivity of urbanization effects to the urban fraction*

The two sensitivity experiments, Urban1 and Urban1_ConsFrac, were downscaled from the GFS_Urban run and GFS_Urban_ConsFrac run, respectively. The differences between the Urban1_ConsFrac run and the NoUrban run indicated the urbanization effects with an exaggerated urban fraction map, which was specified a constant value of 0.4. The effects of urbanization with this exaggerated urban fraction map and the sensitivity of these effects to the urban fraction are discussed in this section.

With the urban fraction map changing to a constant value of 0.4 (Urban1_ConsFrac), the urban fraction in most of the urban areas (Fig. 1b) increases, indicating an expansion of urbanization, while only over the intensive urbanization areas (e.g., some areas in the BTH and YRD) did the urban fraction decrease, by about 0.1–0.4.

The results indicate that the general pattern of the effects of urbanization simulated with the constant urban fraction map is similar to that simulated with the realistic urban fraction map (Figs. 6, 11). Associated with the high urban fraction, the surface temperature (Fig. 11a) increases substantially over all of the urban areas and decreased to the south of the Yangtze River. A similarly dry precipitation belt was apparent over North China along with three wet belts outside the urban areas, as discussed in Section 3.1. With the exaggerated urban fraction, the general pattern does not change (Fig. 11b).

However, there are some differences in the finer details. For example, the reduction in surface latent heat flux (not shown) strengthens with the increase in urban fraction. Therefore, the warming over the three urban areas covers a much larger area and became stronger (Figs. 6a, 11a). In addition, the reduction in evaporation over the north of the YRD area is larger (not shown) than that simulated with the realistic urban fraction map (Fig. 5a), and quite dominant. Meanwhile, the northward mon-

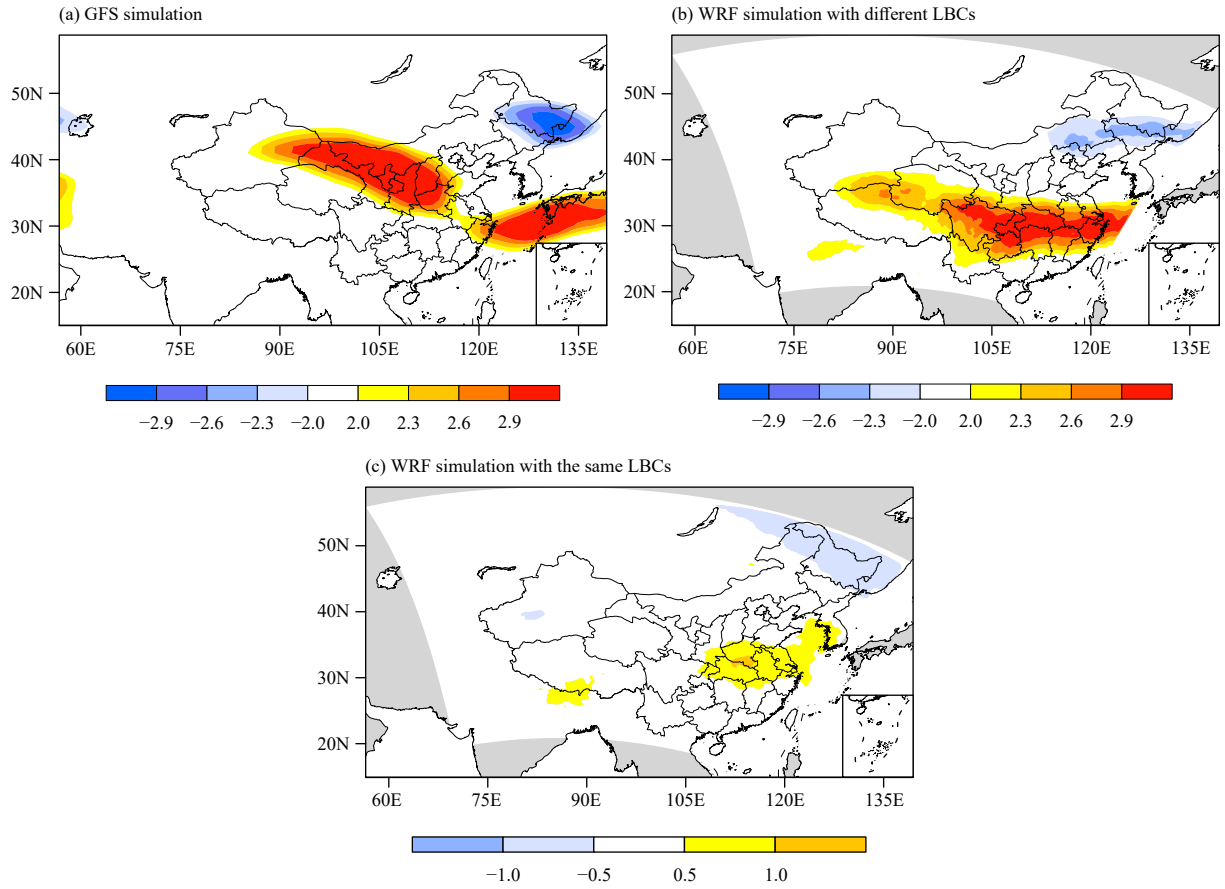

Fig. 10. Urbanization effects on June–July mean zonal wind (m s^{-1}) at 200 hPa: (a) GFS simulation, (b) WRF simulation with different LBCs, and (c) WRF simulation with the same LBCs.

soonal flow becomes weak and shifted to the south, as indicated by a relatively southward monsoonal flow and enhances convergence to the south of the Yangtze River (Fig. 12). As such, the increase in precipitation over the north of the YRD is not as significant as that simulated with the realistic urban fraction map; and meanwhile, the increase in precipitation over the south of the Yangtze River becomes very strong (Figs. 6b, 11b).

4. Conclusions and discussion

In this study, an urban canopy model is coupled to the SSIB land-surface model in both GFS and WRF-ARW v3.7 to explore the large-scale urbanization effect in eastern China. The results with the nested GFS and WRF with/without urbanization show that the large-scale urbanization in eastern China significantly impacts the regional climate. With urbanization, the cloud cover decreases over most urban areas due to reduced evapotranspiration, leading to a decrease in the surface net radiation flux. The surface latent heat flux decreases substantially because of the changes in surface characteristics. To balance the surface energy budget, both the surface sensible heat flux and ground heat flux increase. Accordingly, the surface temperature increases significantly over the urban areas.

With the reduced latent heating in the mid and upper atmosphere over North China where the large-scale urbanization occurrs, and the corresponding change in the temperature gradient in eastern China, a relative descending motion occurrs and the subtropical jet shifts southward, which produce divergence over North China and weakening of the East Asian summer monsoon. The divergence over North China contributes substantially to the warming over rural areas in North China, resulting in a large surface warming pattern that does coincide with the urban regions.

To the south of North China, the anomalous convergence caused by the urbanization induces divergence over North China and the weakened East Asian summer monsoon is dominant, producing changes in cloud and radiation. Since the increase in integrated moisture flux convergence is dominant, precipitation increases significantly over the north of the YRD area and to the south of

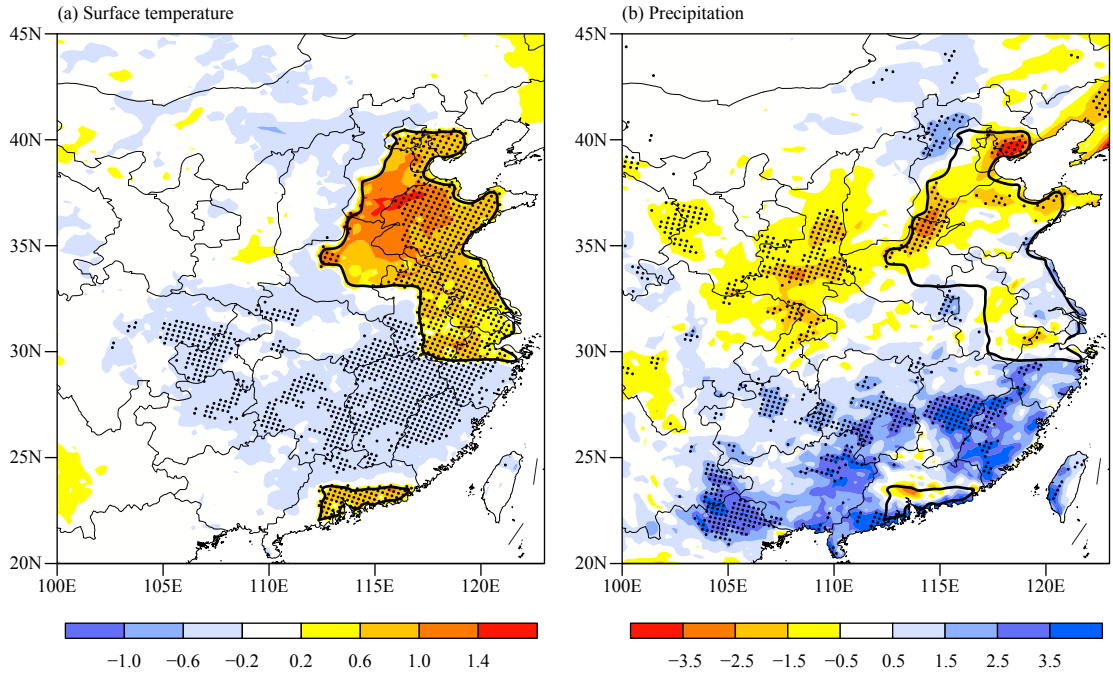

Fig. 11. WRF-simulated June–July urbanization effects on (a) surface temperature (°C) and (b) precipitation (mm day^{-1}) with the constant urban fraction map (0.4). Black dots indicate statistically significant areas at the 90% confidence level according to a *t*-test. The two anomalous regions encircled in black indicate urban areas where the urban fraction is 0.4.

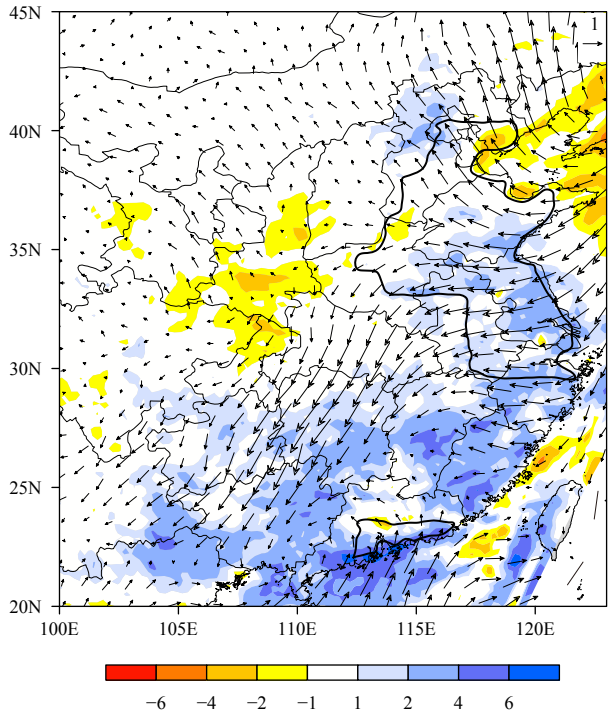

Fig. 12. WRF-simulated June–July urbanization effects on wind at 850 hPa and integrated moisture flux convergence over the whole atmospheric column (mm day^{-1}) with the constant urban fraction map (0.4). The two anomalous regions encircled in black indicate urban areas where the urban fraction is 0.4.

the Yangtze River. Similarly, anomalous convergence to the north of North China leads to significant increases in precipitation. The simulated effects of urbanization on precipitation are generally consistent with previous studies based on observational data (Seto et al., 2012; Niyogi et al., 2017, 2020), which suggest that the impact of urbanization on precipitation depends on where the urbanization has occurred, and rainfall could increase either upwind or downwind.

Urban LULC change affects both surface evapotranspiration and moisture flux convergence (Xue, 1996, 1997). On the one hand, the reduction in evaporation over urban areas weakens (strengthens) the convective available potential energy (convective inhibition) and reduces precipitation (Zhang et al., 2009; Georgescu et al., 2012; Wang et al., 2012, 2015; Feng et al., 2015); while on the other hand, the urban-induced increase in surface temperature and roughness can initiate or enhance local convection, which may lead to an increase in precipitation (Bornstein and Lin, 2000; Rozoff et al., 2003; Shepherd, 2005; Zhang et al., 2010; Cheng and Chan, 2012; Wang et al., 2012; Han et al., 2014). Therefore, the final urbanization effect on precipitation depends on whether the positive or the negative effect is dominant (Wang et al., 2015). Over the coastal areas, such as in the PRD and YRD, the convergence induced by warm surface temperatures could be dominant, offseting the moisture loss due to less evaporation.

As discussed in the introduction, observational data

and modeling studies suggest that the effects of urbanization show complex features, the nature of which depends on the location of the urban area, its size/morphology/intensity, the regional climate, characteristics of rainfall patterns, etc. The urbanization effects in different geographic locations have to be investigated individually. The present study sought to address the issues that may cause the most uncertainty in evaluating the effects of urbanization. Most RCM studies use the same LBCs for both their control and sensitivity runs. This study, with different LBCs for the control and urban sensitivity runs, has revealed that, to investigate large-scale urbanization effects more comprehensively, an RCM nested with a global model may be necessary. Although using different/the same LBCs may produce similar patterns over and around urban areas where the local effect of the land is dominant, they will produce very different results outside the urban areas. That said, within the urban area or nearby areas (20–50 km away from city), the results could be similar with different/the same LBCs, albeit the intensity of the change over and around the urban areas may also bear some differences.

This study also explored the uncertainty of urbanization effects caused by the uncertainty of the urban fraction, which represents the intensity of the urbanization. The results indicated that the effects of urbanization were sensitive to the urban fraction. However, the general pattern of the urbanization effects did not change.

In addition to the LBCs and urban fraction, there are many other sources that may lead to uncertainties in simulating urbanization effects, such as the LULC map, domain size and location, horizontal resolution, model dynamics, and physical parameterizations (Xue et al., 2014; Li et al., 2016). This study was a sensitivity study aimed at investigating the climatic effect and underlying mechanism of large-scale urbanization. For weather forecasting in urban areas, owing to the rapid development of urbanization, the latest information on urbanization may need to be included. Since this study focused on the large-scale features of the effects of urbanization, both the horizontal and temporal resolution was coarse. Experiments with higher resolutions may be needed in the future to explore the finer features of urbanization effects, such as the intensity, frequency, and timing of changes in rainfall. In this research, a total of 18 input urban parameters were used in the urban canopy parameterization scheme. Realistic urban parameter values are difficult to obtain and may vary greatly among different urban areas. Further measurements and analyses are needed to assess the uncertainty caused by these factors.

Acknowledgements. The data used are listed in the references. The authors thank Dr. Ismaila Dialo and Miss Huilin Huang of UCLA for helping the first author to work on the WRF model, and Dr. Kang Yang of Nanjing University for helping the first author to work on the remote sensing dataset. This material is based upon work supported by the National Center for Atmospheric Research (NCAR), which is a major facility sponsored by the NSF under Cooperative Agreement No. 1852977. Computing and data storage resources, including the Cheyenne supercomputer (doi: 10.5065/D6RX99HX), were provided by the Computational and Information Systems Laboratory (CISL) at NCAR. The authors also acknowledge the Texas Advanced Computing Center (TACC) at the University of Texas at Austin for providing high performance computer resources.

REFERENCES

Bornstein, R., and Q. L. Lin, 2000: Urban heat islands and summertime convective thunderstorms in Atlanta: Three case studies. *Atmos. Environ.*, **34**, 507–516, doi: 10.1016/S1352-2310(99)00374-X.

Cao, Q., D. Y. Yu, M. Georgescu, et al., 2016: Impacts of urbanization on summer climate in China: An assessment with coupled land-atmospheric modeling. *J. Geophys. Res. Atmos.*, **121**, 10,505–10,521, doi: 10.1002/2016JD025210.

Cao, Q., Y. P. Liu, M. Georgescu, et al., 2020: Impacts of landscape changes on local and regional climate: A systematic review. *Landsc. Ecol.*, **35**, 1269–1290, doi: 10.1007/s10980-020-01015-7.

Chen, J., A. Liao, L. Chen, et al., 2014: Global Artificial land surface dataset at 30 m resolution (2010). *Digital Journal of Global Change Data Repository*. Available online at http://www.geodoi.ac.cn/edoi.aspx?Id=163. Accessed on 20 December 2021.

Chen, J., A. P. Liao, L. J. Chen, et al., 2017: Content and composition of global artificial land surface dataset at 30 m resolution (2010). *J. Global Change Data Discovery*, **1**, 136–148, doi: 10.3974/geodp.2017.02.02. (in Chinese)

Cheng, F., C. Wang, J. L. Wang, et al., 2011: Trend analysis of building height and total floor space in Beijing, China using ICESat/GLAS data. *Int. J. Remote Sens.*, **32**, 8823–8835, doi: 10.1080/01431161.2010.547531.

Cheng, C. K. M., and J. C. L. Chan, 2012: Impacts of land use changes and synoptic forcing on the seasonal climate over the Pearl River Delta of China. *Atmos. Environ.*, **60**, 25–36, doi: 10.1016/j.atmosenv.2012.06.019.

Cheng, J., S. L. Liang, Y. J. Yao, et al., 2014: A comparative study of three land surface broadband emissivity datasets from satellite data. *Remote Sens.*, **6**, 111–134, doi: 10.3390/rs6010111.

Collins, W. D., P. J. Rasch, B. A. Boville, et al., 2004: Description of the NCAR Community Atmosphere Model (CAM 3.0). NCAR Tech. Note NCAR/TN-464+STR, University Corporation for Atmospheric Research, Boulder, CO, USA, 214 pp.

Cui, Q. Y., Y. Pan, and X. Yang, 2015: Beijing plain area of re-

mote sensing images based on Landsat 8 impermeable layer coverage estimates. *J. Capital Normal Univ. (Nat. Sci. Ed.)*, **36**, 89–92, doi: 10.3969/j.issn.1004-9398.2015.02.019. (in Chinese)

Dee, D. P., S. M. Uppala, A. J. Simmons, et al., 2011: The ERA-Interim reanalysis: Configuration and performance of the data assimilation system. *Quart. J. Roy. Meteor. Soc.*, **137**, 553–597, doi: 10.1002/qj.828.

Ding, C. R., 2013: Building height restrictions, land development and economic costs. *Land Use Policy*, **30**, 485–495, doi: 10.1016/j.landusepol.2012.04.016.

Du, Y., Y. C. Zhang, and Z. Q. Xie, 2009: Location variation of the East Asia subtropical westerly jet and its effect on the summer precipitation anomaly over eastern China. *Chinese J. Atmos. Sci.*, **33**, 581–592, doi: 10.3878/j.issn.1006-9895.2009.03.15. (in Chinese)

Feng, J. M., Y. L. Wang, and Z. G. Ma, 2015: Long-term simulation of large-scale urbanization effect on the East Asian monsoon. *Climatic Change*, **129**, 511–523, doi: 10.1007/s10584-013-0885-2.

Fu, X. S., X. Q. Yang, and X. G. Sun, 2019: Spatial and diurnal variations of summer hourly rainfall over three super city clusters in eastern China and their possible link to the urbanization. *J. Geophys. Res. Atmos.*, **124**, 5445–5462, doi: 10.1029/2019JD030474.

Georgescu, M., A. Mahalov, and M. Moustaoui, 2012: Seasonal hydroclimatic impacts of sun corridor expansion. *Environ. Res. Lett.*, **7**, 034026, doi: 10.1088/1748-9326/7/3/034026.

Han, J.-Y., J.-J. Baik, and H. Lee, 2014: Urban impacts on precipitation. *Asia-Pac. J. Atmos. Sci.*, **50**, 17–30, doi: 10.1007/s13143-014-0016-7.

Han, L. F., Y. P. Xu, L. Yang, et al., 2015: Temporal and spatial change of stream structure in Yangtze River Delta and its driving forces during 1960s-2010s. *Acta Geogr. Sin.*, **70**, 819–827, doi: 10.11821/dlxb201505012. (in Chinese)

Hong, S.-Y., and J.-O. J. Lim, 2006: The WRF single-moment 6-class microphysics scheme (WSM6). *J. Korean Meteor. Soc.*, **42**, 129–151.

Hong, S.-Y., Y. Noh, and J. Dudhia, 2006: A new vertical diffusion package with an explicit treatment of entrainment processes. *Mon. Wea. Rev.*, **134**, 2318–2341, doi: 10.1175/MWR3199.1.

Hu, Y. H., G. S. Jia, C. Pohl, et al., 2015: Improved monitoring of urbanization processes in China for regional climate impact assessment. *Environ. Earth Sci.*, **73**, 8387–8404, doi: 10.1007/s12665-014-4000-4.

Jackson, T. L., J. J. Feddema, K. W. Oleson, et al., 2010: Parameterization of urban characteristics for global climate modeling. *Ann. Assoc. Am. Geogr.*, **100**, 848–865, doi: 10.1080/00045608.2010.497328.

Jia, G. S., R. H. Xu, Y. H. Hu, et al., 2015: Multi-scale remote sensing estimates of urban fractions and road widths for regional models. *Climatic Change*, **129**, 543–554, doi: 10.1007/s10584-014-1114-3.

Jiang, Z. H., and Y. Li, 2014: Impact of urbanization in different regions of eastern China on precipitation and its uncertainty. *J. Trop. Meteor.*, **30**, 601–611, doi: 10.3969/j.issn.1004-4965.2014.04.001. (in Chinese)

Jin, M. L., R. E. Dickinson, and D. Zhang, 2005: The footprint of urban areas on global climate as characterized by MODIS. *J. Climate*, **18**, 1551–1565, doi: 10.1175/JCLI3334.1.

Kain, J. S., 2004: The Kain–Fritsch convective parameterization: An update. *J. Appl. Meteor.*, **43**, 170–181, doi: 10.1175/1520-0450(2004)043<0170:TKCPAU>2.0.CO;2.

Kaufmann, R. K., K. C. Seto, A. Schneider, et al., 2007: Climate response to rapid urban growth: Evidence of a human-induced precipitation deficit. *J. Climate*, **20**, 2299–2306, doi: 10.1175/JCLI4109.1.

Li, W. K., W. D. Guo, Y. K. Xue, et al., 2016: Sensitivity of a regional climate model to land surface parameterization schemes for East Asian summer monsoon simulation. *Climate Dyn.*, **47**, 2293–2308, doi: 10.1007/s00382-015-2964-8.

Li, W. P., Y. K. Xue, and I. Poccard, 2007: Numerical investigation of the impact of vegetation indices on the variability of West African summer monsoon. *J. Meteor. Soc. Japan*, **85A**, 363–383, doi: 10.2151/jmsj.85A.363.

Li, Z. Q., L. L. Song, H. Ma, et al., 2017: Observed surface wind speed declining induced by urbanization in East China. *Climate Dyn.*, **50**, 735–749, doi: 10.1007/s00382-017-3637-6.

Li, Z., Z. W. Yan, K. Tu, et al., 2015: Changes of precipitation and extremes and the possible effect of urbanization in the Beijing metropolitan region during 1960–2012 based on homogenized observations. *Adv. Atmos. Sci.*, **32**, 1173–1185, doi: 10.1007/s00376-015-4257-x.

Liao, W. L., D. G. Wang, X. P. Liu, et al., 2017: Estimated influence of urbanization on surface warming in eastern China using time-varying land use data. *Int. J. Climatol.*, **37**, 3197–3208, doi: 10.1002/joc.4908.

Liu, J. K., Z. Q. Gao, L. L. Wang, et al., 2018: The impact of urbanization on wind speed and surface aerodynamic characteristics in Beijing during 1991–2011. *Meteor. Atmos. Phys.*, **130**, 311–324, doi: 10.1007/s00703-017-0519-8.

Liu, Q., L. Z. Wang, Y. Qu, et al., 2013: Preliminary evaluation of the long-term GLASS albedo product. *Int. J. Digit. Earth*, **6**, 69–95, doi: 10.1080/17538947.2013.804601.

Liu, Z. X., 2013: Assessing the urbanization effects by applying an urban canopy model and coupling it with weather research and forecasting model. Ph.D. dissertation, Peking University, Beijing, 204 pp. (in Chinese)

Lo, J. C. F., A. K. H. Lau, F. Chen, et al., 2007: Urban modification in a mesoscale model and the effects on the local circulation in the Pearl River delta region. *J. Appl. Meteor. Climatol.*, **46**, 457–476, doi: 10.1175/JAM2477.1.

Ma, H. Y., Z. H. Jiang, J. Song, et al., 2016: Effects of urban land-use change in East China on the East Asian summer monsoon based on the CAM5.1 model. *Climate Dyn.*, **46**, 2977–2989, doi: 10.1007/s00382-015-2745-4.

Meng, C. L., and Y. J. Dai, 2013: Development and verification of a bulk urbanized land surface model. *Chinese J. Atmos. Sci.*, **37**, 1297–1308, doi: 10.3878/j.issn.1006-9895.2013.12185. (in Chinese)

Miao, S. G., F. Chen, M. A. LeMone, et al., 2008: An observational and modeling study of characteristics of urban heat island and boundary layer structures in Beijing. *J. Appl. Meteor. Climatol.*, **48**, 484–501, doi: 10.1175/2008JAMC1909.1.

Miao, S. G., J. X. Dou, F. Chen, et al., 2012: Analysis of observations on the urban surface energy balance in Beijing. *Sci. China Earth Sci.*, **55**, 1881–1890, doi: 10.1007/s11430-012-

4411-6.

Niyogi, D., M. Lei, C. Kishtawal, et al., 2017: Urbanization impacts on the summer heavy rainfall climatology over the Eastern United States. *Earth Interact.*, **21**, 1–17, doi: 10.1175/EI-D-15-0045.1.

Niyogi, D., K. K. Osuri, N. K. R. Busireddy, et al., 2020: Timing of rainfall occurrence altered by urban sprawl. *Urban Climate*, **33**, 100643, doi: 10.1016/j.uclim.2020.100643.

Oke, T. R., 1979: Review of Urban Climatology 1973–1976. WMO Technical Note No. 169, WMO No. 539. World Meteorological Organization, Geneva. Available online at https://library.wmo.int/index.php?lvl=notice_display&id=6310#.YYNBIeR7kuV.

Oleson, K. W., G. B. Bonan, J. Feddema, et al., 2008: An urban parameterization for a global climate model. Part I: Formulation and Evaluation for Two Cities. *J. Appl. Meteor. Climatol.*, **47**, 1038–1060, doi: 10.1175/2007JAMC1597.1.

Peng, S. S., S. L. Piao, P. Ciais, et al., 2012: Surface urban heat island across 419 global big cities. *Environ. Sci. Technol.*, **46**, 696–703, doi: 10.1021/es2030438.

Rozoff, C. M., W. R. Cotton, and J. O. Adegoke, 2003: Simulation of St. Louis, Missouri, land use impacts on thunderstorms. *J. Appl. Meteor.*, **42**, 716–738, doi: 10.1175/1520-0450(2003)042<0716:SOSLML>2.0.CO;2.

Saha, S., S. Moorthi, H.-L. Pan, et al., 2010: The NCEP climate forecast system reanalysis. *Bull. Amer. Meteor. Soc.*, **91**, 1015–1057, doi: 10.1175/2010BAMS3001.1.

Sato, T., and Y. K. Xue, 2013: Validating a regional climate model's downscaling ability for East Asian summer monsoonal interannual variability. *Climate Dyn.*, **41**, 2411–2426, doi: 10.1007/s00382-012-1616-5.

Seto, K. C., A. Reenberg, C. G. Boone, et al., 2012: Urban land teleconnections and sustainability. *Proc. Natl. Acad. Sci. USA*, **109**, 7687–7692, doi: 10.1073/pnas.1117622109.

Shepherd, J. M., 2005: A review of current investigations of urban-induced rainfall and recommendations for the future. *Earth Interact.*, **9**, 1–27, doi: 10.1175/EI156.1.

Skamarock, W. C., J. B. Klemp, J. Dudhia, et al., 2008: A description of the advanced research WRF version 3. NCAR Tech. Note NCAR/TN-475+STR, National Center for Atmospheric Research, Boulder, Colorado, USA, 113 pp.

Song, X. M., J. Y. Zhang, A. Aghakouchak, et al., 2014: Rapid urbanization and changes in spatiotemporal characteristics of precipitation in Beijing metropolitan area. *J. Geophys. Res. Atmos.*, **119**, 11250–11271, doi: 10.1002/2014JD022084.

Sun, S. F., and Y. K. Xue, 2001: Implementing a new snow scheme in Simplified Simple Biosphere Model (SSiB). *Adv. Atmos. Sci.*, **18**, 335–354, doi: 10.1007/BF02919314.

Wang, J., J. M. Feng, Z. W. Yan, et al., 2012: Nested high-resolution modeling of the impact of urbanization on regional climate in three vast urban agglomerations in China. *J. Geophys. Res. Atmos.*, **117**, D21103, doi: 10.1029/2012JD018226.

Wang, J., J. M. Feng, and Z. W. Yan, 2015: Potential sensitivity of warm season precipitation to urbanization extents: Modeling study in Beijing-Tianjin-Hebei urban agglomeration in China. *J. Geophys. Res. Atmos.*, **120**, 9408–9425, doi: 10.1002/2015JD023572.

Wang, W.-C., Z. M. Zeng, and T. R. Karl, 1990: Urban heat islands in China. *Geophys. Res. Lett.*, **17**, 2377–2380, doi: 10.1029/GL017i013p02377.

Wang, X. M., J. B. Liao, J. Zhang, et al., 2013: A numeric study of regional climate change induced by urban expansion in the Pearl River Delta, China. *J. Appl. Meteor. Climatol.*, **53**, 346–362, doi: 10.1175/JAMC-D-13-054.1.

Wang, Y. W., and W. M. Jiang, 2009: Numerical study on development of a multilayer urban canopy model. *Acta Meteor. Sinica*, **67**, 1013–1024, doi: 10.11676/qxxb2009.098. (in Chinese)

Wu, J., J. L. Zha, and D. M. Zhao, 2016: Estimating the impact of the changes in land use and cover on the surface wind speed over the East China Plain during the period 1980–2011. *Climate Dyn.*, **46**, 847–863, doi: 10.1007/s00382-015-2616-z.

Wu, K., and X. Q. Yang, 2013: Urbanization and heterogeneous surface warming in eastern China. *Chinese Sci. Bull.*, **58**, 1363–1373, doi: 10.1007/s11434-012-5627-8.

Xue, Y., K. N. Liou, and A. Kasahara, 1990: Investigation of the biogeophysical feedback on the African climate using a two-dimensional model. *J. Climate*, **3**, 337–352, doi: 10.1175/1520-0442(1990)003<0337:IOBFOT>2.0.CO;2.

Xue, Y., P. J. Sellers, J. L. Kinter, et al., 1991: A simplified biosphere model for global climate studies. *J. Climate*, **4**, 345–364, doi: 10.1175/1520-0442(1991)004<0345:ASBMFG>2.0.CO;2.

Xue, Y. K., 1996: The impact of desertification in the Mongolian and the Inner Mongolian Grassland on the regional climate. *J. Climate*, **9**, 2173–2189, doi: 10.1175/1520-0442(1996)009<2173:TIODIT>2.0.CO;2.

Xue, Y. K., 1997: Biosphere feedback on regional climate in tropical North Africa. *Quart. J. Roy. Meteor. Soc.*, **123**, 1483–1515, doi: 10.1002/qj.49712354203.

Xue, Y. K., H.-M. H. Juang, W. P. Li, et al., 2004: Role of land surface processes in monsoon development: East Asia and West Africa. *J. Geophys. Res. Atmos.*, **109**, D03105, doi: 10.1029/2003JD003556.

Xue, Y. K., F. De Sales, R. Vasic, et al., 2010: Global and seasonal assessment of interactions between climate and vegetation biophysical processes: A GCM study with different land–vegetation representations. *J. Climate*, **23**, 1411–1433, doi: 10.1175/2009JCLI3054.1.

Xue, Y. K., Z. Janjic, J. Dudhia, et al., 2014: A review on regional dynamical downscaling in intraseasonal to seasonal simulation/prediction and major factors that affect downscaling ability. *Atmos. Res.*, **147–148**, 68–85, doi: 10.1016/j.atmosres.2014.05.001.

Xue, Y. K., I. Diallo, W. K. Li, et al., 2018: Spring land surface and subsurface temperature anomalies and subsequent downstream late spring-summer droughts/floods in North America and East Asia. *J. Geophys. Res. Atmos.*, **123**, 5001–5019, doi: 10.1029/2017JD028246.

Yan, Z. W., J. Wang, J. J. Xia, et al., 2016: Review of recent studies of the climatic effects of urbanization in China. *Adv. Climate Change Res.*, **7**, 154–168, doi: 10.1016/j.accre.2016.09.003.

Yang, P., G. Y. Ren, and W. D. Liu, 2013: Spatial and temporal characteristics of Beijing urban heat island intensity. *J. Appl. Meteor. Climatol.*, **52**, 1803–1816, doi: 10.1175/jamc-d-12-0125.1.

Zha, J. L., J. Wu, and D. M. Zhao, 2017: Effects of land use and

cover change on the near-surface wind speed over China in the last 30 years. *Prog. Phys. Geog.*, **41**, 46–47, doi: 10.1177/0309133316663097.

Zhang, C. L., F. Chen, S. G. Miao, et al., 2009: Impacts of urban expansion and future green planting on summer precipitation in the Beijing metropolitan area. *J. Geophys. Res. Atmos.*, **114**, D02116, doi: 10.1029/2008JD010328.

Zhang, N., Z. Q. Gao, X. M. Wang, et al., 2010: Modeling the impact of urbanization on the local and regional climate in Yangtze River Delta, China. *Theor. Appl. Climatol.*, **102**, 331–342, doi: 10.1007/s00704-010-0263-1.

Zhang, Y., J. A. Smith, L. F. Luo, et al., 2014: Urbanization and rainfall variability in the Beijing metropolitan region. *J. Hydrometeorl.*, **15**, 2219–2235, doi: 10.1175/JHM-D-13-0180.1.

Zhao, D. M., and J. Wu, 2017: The influence of urban surface expansion in China on regional climate. *J. Climate*, **30**, 1061–1080, doi: 10.1175/JCLI-D-15-0604.1.

Zhou, D. C., S. Q. Zhao, L. X. Zhang, et al., 2015: The footprint of urban heat island effect in China. *Sci. Rep.*, **5**, 11160, doi: 10.1038/srep11160.

Tech & Copy Editor: Mengyuan CHEN